# Research on strategy of load-side resonant soft-switching inverter based on interconnection and damping assignment-passivity based control

YAJING ZHANG⊠, HUANCHEN ZHANG, JIANGUO LI, JIUHE WANG

*School of Automation, Beijing Information Science & Technology University*
*No.12 Qinghe Xiaoying East Road, Haidian District, Beijing, China*
e-mail: *{⊠ zhangyajing/2021020432/lijianguo}@bistu.edu.cn, wjhyhrwm@163.com*

**Abstract:** Soft-switching technologies can effectively solve the problem of switching losses caused by increasing switching frequency of grid-connected inverters. As a branch of soft-switching technologies, load-side resonant soft-switching is a hotspot for applications of high-frequency inverters, because it has the advantage of achieving soft-switching without using additional components. However, the traditional PI control strategy based on the linear model is prone to destabilization and non-robust dynamic performance when large signal perturbation occurs. In this paper, a novel Passivity-Based Control (PBC) method is proposed to improve the dynamic performance of load-side resonant soft-switching grid-connected inverter. Besides, the model based on the Port Controlled Hamiltonian (PCH) model of the soft switching inverter is carried out, and the passivity-based controller is designed based on the established model using the way of interconnection and damping assignment-passivity based control (IDA-PBC). Both stable performance and dynamic performance of the load-side resonant soft-switching inverter can be improved over the whole operating range. Finally, a 750 W load-side resonant soft-switching inverter simulation model is built and the output performance is compared with the traditional PI control strategy under stable and dynamic conditions. The simulation results show that the proposed control strategy reduces the harmonic distortion rate and improves the quality of the output waveforms.

**Key words:** boundary current mode, interconnection and damping assignment-passivity based control, single-phase grid-connected inverter, switching loss

# 1. Introduction

In recent years, technologies related to the generation of renewable energies have developed rapidly. As an important part of the generation system, the inverter not only converts DC power into AC power and transmits it to the grid, but also affects the stability and the efficiency of energy conversion of the whole system. Therefore, the innovation of inverter technologies has become an important force to promote the development of the generation of renewable energies. At present, high frequency, miniaturization, digitalization are the hot spots and important directions of inverter technologies. The increasing switching frequency of inverters can reduce the size of passive filter devices, lower the corresponding manufacturing cost, increase the power density of inverters, and improve the quality of waveforms [1]. However, as the switching frequency increases, the switching losses of the switches also increase and electromagnetic interference worsens.

High-frequency inverter technologies have developed rapidly in recent years, and the classification of soft-switching inverters according to the position of resonance process has two types: DC-side resonant soft switches and AC-side resonant soft switches. Among them, DC-side resonant soft switches can be divided into two types: DC-side series resonant switches and DC-side parallel resonant switches; AC-side resonant soft switches can be further divided into two types: pole resonant soft switches and load-side resonant soft switches.

The DC-side resonant soft switches were developed from the basic Resonant DC-Link Inverter (RDCLI) circuit proposed by Professor Divan, then a large number of DC-side parallel resonant circuits were proposed based on the idea of DC-side parallel resonant switches [2,3]. The difference between DC-side series resonant switches and DC-side parallel resonant switches lies in the different forms of connection between the resonant auxiliary circuit and the main circuit. Both of them work on the theory of soft switching by adding a resonant loop on the DC side of the inverter to reduce the voltage of the inverter's switches to zero. Papers [4,5] showed the applications of dc-side resonant soft-switching technology in Photo Voltaic (PV) systems.

The pole resonant soft switching circuit has a resonant loop that is independent of the power circuit and is connected at the midpoint of the bridge of switches. The advantage of the pole resonant soft-switching circuit is that the auxiliary circuit operates only for a very short time during the whole switching cycle, thus contributing to the reduction of the losses of the auxiliary circuit. Papers [6–8] belonged to the applications of the pole resonant soft-switching technology in photovoltaic systems. Paper [6] successfully applied pole resonant soft switching in inverters, but two auxiliary switches were required for each bridge of switches. To reduce the complexity of the auxiliary circuit, a new topology was proposed in paper [7], but one auxiliary switch and two diodes were still required for each bridge of switches.

In recent years, a class of soft-switching technologies without resonant auxiliary circuits has been developed based on pole resonant soft-switching, which is called load-side resonant soft-switching. Unlike the traditional soft-switching technologies, it forms a resonant circuit through the parasitic capacitors of the switches and the load-side inductor without adding additional auxiliary components, which creates conditions for the zero-voltage conduction of the switches by achieving the bidirectional flow of the inductor current in one switching cycle, thus greatly reducing the switching losses [9]. Load-side resonant soft switching was first used in DC-DC converters with mature applications. Subsequently, it was used in a large number of power factor correction (PFC) circuits [10–12]. In recent years, the load-side resonant soft-switching technology has been successfully applied in low-power inverters [13–15].

In the control of load-side resonant soft-switching inverters, paper [16] used Proportional-Integral (PI) control as the control method of load-side resonant soft-switching in boundary current mode, but the traditional PI control is based on the linear model of the system, which has non-robust dynamic performance when large signal perturbations are encountered and makes it difficult to keep the system stable. As inverters are non-linear systems, applying a linear control strategy such as PI control to a non-linear system is limited. The physical meaning of passivity is closely related to the Lyapunov function and is an important concept in network theory. Interconnection and Damping Assignment-Passivity Based Control (IDA-PBC) is a new theory of passivity-based control based on Hamiltonian systems proposed by Professor Ortega [17, 18], which is a control strategy from the perspective of the energies in the system, which can simplify design process of the controller in nonlinear systems and have advantages of no overshoot, high stability and good robustness. At present, the IDA-PBC control strategy was applied in motor control, power electronics devices, and power systems successfully [19, 20].

In this paper, we design the passivity-based controller based on the theory of IDA-PBC in order to improve the performance of load-side resonant soft-switching single-phase grid-connected inverters. The paper is structured as follows: Section 2 briefly describes the operation of a load-side resonant soft-switching single-phase grid-connected inverter in boundary current modulation mode. Then Section 3 models the load-side resonant soft-switched single-phase grid-connected inverter according to the Port Controlled Hamiltonian (PCH) model in Passivity-Based Control (PBC) theory, designs the passivity-based controller using the IDA-PBC approach and then demonstrates the passive nature of the whole system. In Section 4 a PSIM simulation model is built to compare the performance of the system under PI control and PBC in stable and dynamic state. Finally, in Section 5 the conclusion of the paper is given.

## 2. Topology and operation principal of the load-side resonant soft-switching inverter

As shown in Fig. 1, the topology of the load-side resonant soft-switch inverter is mainly divided into a full-bridge circuit composed of four switches, a filter circuit composed of resonant inductor $L_1$, filter capacitor $C$ and filter inductor $L_2$, where $u_d$ is the input voltage of DC side, and $u_g$ is the voltage of grid. In this paper, inverter operates in boundary current modulation mode, $S_1$ and $S_2$ are high frequency switches, $S_3$ and $S_4$ are power frequency switches.

The operating principle of the load-side resonant soft switch is shown in Fig. 1, taking the positive half-cycle of the inverter's industrial frequency as an example. Process (1) is the charging stage of resonant inductor $L_1$, and process (2) is the renewal stage to achieve high-frequency resonance at the midpoint of the bridge of switches to achieve zero-voltage conduction of switch $S_2$. Then, the resonant inductor current $i_{L1}$ drops to zero even flows in the reverse direction in every switching cycle to create high-frequency resonance process (3) at the midpoint of the bridge of switches to achieve zero-voltage turn-on of switch $S_1$. The load-side resonant soft switch can be realized by setting the envelope of resonant inductor current $i_{L1}$ to achieve.

The equations for the upper and lower limits of the envelope of the inductance current $i_{L1}$ are shown as:

$I_o \sin wt > 0$:

$$\begin{cases} i_{up} = 2I_o \sin wt + \Delta I \\ i_{down} = -\Delta I \end{cases}, \tag{1}$$

$I_o \sin wt < 0$:

$$\begin{cases} i_{\text{up}} = \Delta I \\ i_{\text{down}} = 2I_o \sin wt - \Delta I \end{cases} . \tag{2}$$



High frequency bridge
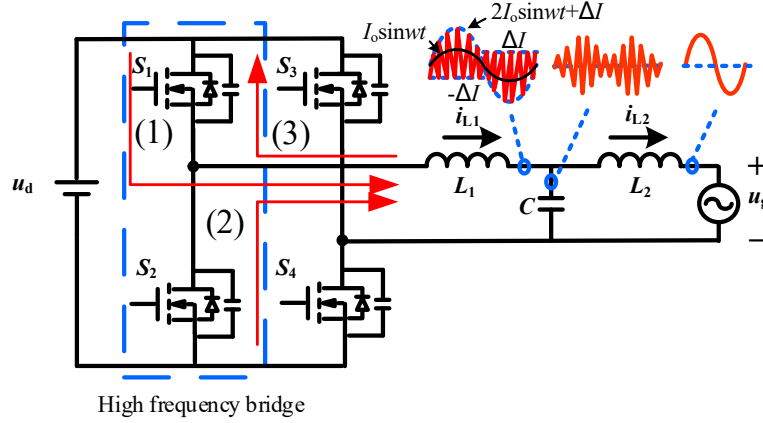
Fig. 1. Topology of load-side resonant soft-switched single-phase grid-connected inverter

# 3. Implementation of the proposed IDA-PBC based resonant soft-switching single-phase grid-connected inverter

## 3.1. Mathematical model of the resonant soft-switching single-phase grid-connected inverter

From the variables in the topology in Fig. 1, the KVL and KCL equations for the load resonant soft-switched single-phase grid-connected inverter in boundary current mode can be expressed as

$$\begin{cases} L_1 \dfrac{di_{\text{L1}}}{dt} + u_{\text{C}} = Su_{\text{d}} \\ L_2 \dfrac{di_{\text{L2}}}{dt} - u_{\text{C}} = -u_{\text{g}} \\ C \dfrac{du_{\text{C}}}{dt} - i_{\text{L1}} + i_{\text{L2}} = 0 \end{cases}, \tag{3}$$

where $S$ is the switching parameter. Fetching state variables $\boldsymbol{x} = [x_1, x_2, x_3]^{\text{T}} = [L_1 i_{\text{L1}}, L_2 i_{\text{L2}}, Cu_{\text{C}}]^{\text{T}}$, and defining the energy storage function of the system as the sum of the magnetic energy of inductors $L_1$ and $L_2$ and the electrical energy of capacitor $C$. The specific expression is

$$\boldsymbol{H(x)} = \frac{1}{2L_1}x_1^2 + \frac{1}{2L_2}x_2^2 + \frac{1}{2C}x_3^2 = \frac{1}{2}\boldsymbol{x}^{\text{T}}\boldsymbol{D}^{-1}\boldsymbol{x}, \tag{4}$$

where

$$D^{-1} = \begin{bmatrix} \dfrac{1}{L_1} & 0 & 0 \\ 0 & \dfrac{1}{L_2} & 0 \\ 0 & 0 & \dfrac{1}{C} \end{bmatrix}. \tag{5}$$

The partial derivatives of the energy storage function $H(x)$ with respect to $x$ are:

$$\frac{\partial H(x)}{\partial x_1} = \frac{x_1}{L_1}, \quad \frac{\partial H(x)}{\partial x_2} = \frac{x_2}{L_2}, \quad \frac{\partial H(x)}{\partial x_3} = \frac{x_3}{C},$$

respectively. The general model of PCH is

$$\dot{x} = (J(x) - R(x))\frac{\partial H(x)}{\partial x} + g(x)u, \tag{6}$$

where: $J(x)$ is the interconnection matrix, $J(x) = J(x)^{\mathrm{T}}$, $R(x)$ is the dissipation matrix, and $g(x)u$ is the external supply.

Thus, the model of the resonant soft-switching single-phase grid-connected inverter based on PCH is shown as

$$\begin{bmatrix} x_1 \\ x_2 \\ x_3 \end{bmatrix} = \begin{bmatrix} 0 & 0 & -1 \\ 0 & 0 & 1 \\ 1 & -1 & 0 \end{bmatrix} \begin{bmatrix} \dfrac{x_1}{L_1} \\ \dfrac{x_2}{L_2} \\ \dfrac{x_3}{C} \end{bmatrix} + \begin{bmatrix} Su_{\mathrm{d}} \\ -u_{\mathrm{g}} \\ 0 \end{bmatrix}. \tag{7}$$

## 3.2. Controller design of the resonant soft-switching single-phase grid-connected inverter based on IDA-PBC

Before applying the passivity-based control to load side soft-switching inverter, the desired state variables of the system are given as follow:

$$x^* = \begin{bmatrix} x_1^* & x_2^* & x_3^* \end{bmatrix}^{\mathrm{T}} = \begin{bmatrix} L_1 i_{\mathrm{L1}}^* & L_2 i_{\mathrm{L2}}^* & C u_{\mathrm{C}}^* \end{bmatrix}^{\mathrm{T}}. \tag{8}$$

To make the PCH system asymptotically stable at the equilibrium point, the desired energy function $H_{\mathrm{d}}(x)$ is constructed after adding feedback control. The desired energy function is defined as

$$H_{\mathrm{d}}(x) = H(x) + H_{\mathrm{a}}x, \tag{9}$$

where $H_{\mathrm{a}}(x)$ denotes the energies that are injected into the system by passivity-based controller, and the PCH system that is expected to be stable at $x^*$ after adding feedback control becomes

$$\dot{x} = [J_{\mathrm{d}}x - R_{\mathrm{d}}x]\frac{\partial H_{\mathrm{d}}x}{\partial x}. \tag{10}$$

The relevant parameters in Eq. (10) are shown as:

$$J_{\mathrm{d}}(x) = J(x) + J_{\mathrm{a}}x, \tag{11}$$

$$J_{\mathrm{a}}x = \begin{bmatrix} 0 & -b & 0 \\ b & 0 & 0 \\ 0 & 0 & 0 \end{bmatrix}, \tag{12}$$

$$R_{\mathrm{d}}(x) = R(x) + R_{\mathrm{a}}x \quad , \tag{13}$$

$$\boldsymbol{R}_a\boldsymbol{x} = \begin{bmatrix} r_1 & 0 & 0 \\ 0 & 0 & 0 \\ 0 & 0 & 0 \end{bmatrix}, \tag{14}$$

where: $\boldsymbol{J}_d(\boldsymbol{x})$ is the desired interconnection matrix, $\boldsymbol{J}_a(\boldsymbol{x})$ is the interconnection matrix of the control, and $b$ is the interconnection coefficient. $\boldsymbol{R}_d(\boldsymbol{x})$ is the desired dissipation matrix, $\boldsymbol{R}_a(\boldsymbol{x})$ is the dissipation matrix of the control, $r_1 > 0$ is the damping factor.

From Eq. (6) and Eq. (10), the following equation can be obtained:

$$(\boldsymbol{J}_d(\boldsymbol{x}) - \boldsymbol{R}_d(\boldsymbol{x}))K(\boldsymbol{x}) = -(\boldsymbol{J}_a(\boldsymbol{x}) - \boldsymbol{R}_a(\boldsymbol{x}))\frac{\partial H(\boldsymbol{x})}{\partial \boldsymbol{x}} + \boldsymbol{g}(\boldsymbol{x})\boldsymbol{u}, \tag{15}$$

where

$$K(\boldsymbol{x}) = \frac{\partial \boldsymbol{H}_a(\boldsymbol{x})}{\partial \boldsymbol{x}}.$$

We can construct the PCH system of Eq. (6) into the form shown in Eq. (10) when the parameters in Eq. (15) satisfy the following requirements – structural conservation of the system.

We can assume that the structure of system is conserved when the parameters of system satisfy the following equation:

$$\begin{cases} \boldsymbol{J}_d(\boldsymbol{x}) = -\boldsymbol{J}_d(\boldsymbol{x})^T \\ \boldsymbol{R}_d(\boldsymbol{x}) = \boldsymbol{R}_d(\boldsymbol{x})^T \geq 0 \end{cases}. \tag{16}$$

In this paper,

$$\boldsymbol{J}_d(\boldsymbol{x}) = \begin{bmatrix} 0 & -b & -1 \\ b & 0 & 1 \\ 1 & -1 & 0 \end{bmatrix}, \quad \boldsymbol{R}_d(\boldsymbol{x}) = \begin{bmatrix} r_1 & 0 & 0 \\ 0 & 0 & 0 \\ 0 & 0 & 0 \end{bmatrix},$$

where $r_1 > 0$.

The relevant parameters satisfy the requirement for structural conservation of the system.

Integrability

$$\frac{\partial K(\boldsymbol{x})}{\partial \boldsymbol{x}} = \left(\frac{\partial K(\boldsymbol{x})}{\partial \boldsymbol{x}}\right)^T. \tag{17}$$

Existence of closed-loop stability points

$$K(\boldsymbol{x}^*) = -\frac{\partial H(\boldsymbol{x})}{\partial \boldsymbol{x}}|_{\boldsymbol{x}=\boldsymbol{x}^*}. \tag{18}$$

Lyapunov stability

$$\frac{\partial H_d^2(\boldsymbol{x})}{\partial \boldsymbol{x}^2}|_{\boldsymbol{x}=\boldsymbol{x}^*} > 0. \tag{19}$$

The parameters in this paper meet the requirements of integrability, existence of closed-loop stability points, and Lyapunov stability. The relevant proofs are easily calculated from the parameters given in the paper, so they are not given in detail in this paper.

After the discussion above, the parameters given in this paper meet the requirements of constructing Eq. (10), and the control rate of the switching tube can be obtained after substituting the relevant parameters into Eq. (15) as follows:

$$C = \frac{u_C^* + r_1\left(i_{L1}^* - i_{L1}\right) + b\left(i_{L2}^* - i_{L2}\right)}{u_d}, \tag{20}$$

where the control rate $C$ is the reference value of the peak of resonant inductor current $i_{L1}$ sinusoidal envelope calculated by the passivity-based controller.

### 3.3. Passivity-based stability criterion of resonant soft-switching single-phase grid-connected inverter

From Eq. (3) the load-side resonant soft-switched single-phase grid-connected inverter model equation can be derived as follows:

$$
\begin{cases}
L_1 \dfrac{\mathrm{d}i_{L1}}{\mathrm{d}t} = -u_C + Su_d \\[2mm]
L_2 \dfrac{\mathrm{d}i_{L2}}{\mathrm{d}t} = u_C - u_g \\[2mm]
C \dfrac{\mathrm{d}u_C}{\mathrm{d}t} = i_{L1} - i_{L2}
\end{cases}
\tag{21}
$$

Multiplying the first equation in Eq. (21) by $i_{L1}$, the second equation by $i_{L2}$, and the third equation by $u_C$ yields the power equation of the system as

$$
\frac{\mathrm{d}}{\mathrm{d}t}\left( \underbrace{\frac{1}{2}L_1 i_{L1}^2 + \frac{1}{2}L_2 i_{L2}^2}_{H_L(t)} + \underbrace{\frac{1}{2}Cu_c^2}_{H_C(t)} \right) = Su_d i_{L1} - u_g i_{L2},
\tag{22}
$$

where $H_C(t)$ is the electric field energy stored in the capacitor and $H_L(t)$ is the electromagnetic energy stored in the inductors. From this, the energy function of the system can be deduced as

$$
\underbrace{H(t)}_{\text{Moment energy of } t} = \underbrace{H(0)}_{\text{Initial energy}} + \underbrace{S \int_0^t u_d i_{L1}\mathrm{d}\tau}_{\text{Supplied energy}} - \underbrace{\int_0^t u_g i_{L2}\mathrm{d}\tau}_{\text{Dissipated energy}}.
\tag{23}
$$

$H(t) = H_L(t) + H_C(t)$ is the total energy of the system, $\tau$ is the integration time constant, since $u_g i_{L2} > 0$, the following dissipation inequality is obtained:

$$
H(t) - H(0) < S \int_0^t u_d i_{L1}\mathrm{d}\tau.
\tag{24}
$$

Therefore, the proposed PBC based controller is asymptotically stable and the system is strictly passive.

### 3.4. Simulation verifications and analysis

In this paper, a simulation model with a power of 750 W is built based on PSIM to verify the proposed PBC strategy, and the schematic of PBC is shown in Fig. 2. The DC-side input voltage $u_d$ is 380 V, the peak of grid voltage $u_g$ is 311 V, the frequency is 50 Hz, and the circuit simulation parameters are shown in Table. 1.

Table 1. Parameters of the simulation

| Symbol | Quantity | Magnitude |
|--------|----------|-----------|
| $i_{L2}^*$ | Desired output current | 4.8 A |
| $L_1$ | Resonant inductor | 150 μH |
| $L_2$ | Filter inductor | 3 mH |
| $C$ | Filter capacitor | 0.56 μF |
| $r_1$ | Damping factor | 75 Ω |
| $b$ | Interconnection coefficient | 137 |
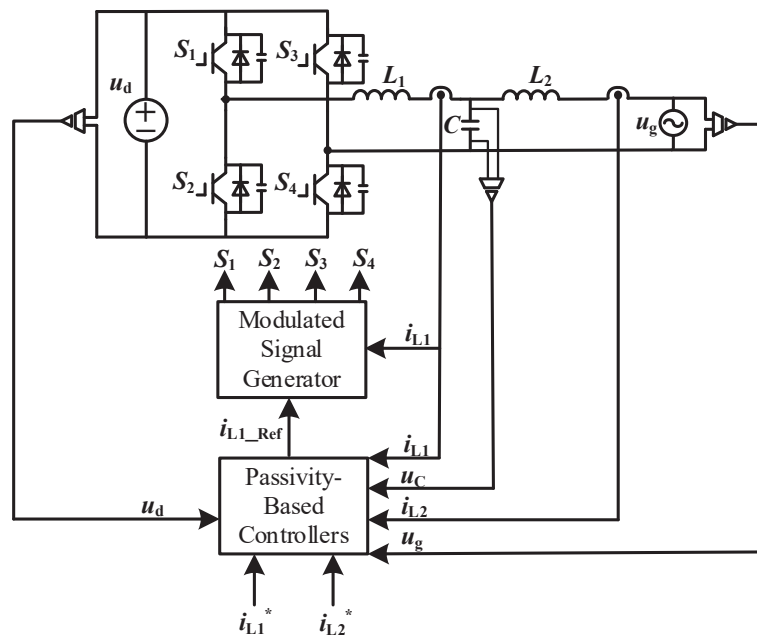


Fig. 2. Schematic diagram of passivity-based control

## 3.5. Stable-state simulation analysis

Parameters of PI control used for comparison are $P = 5$ and $I = 0.001$ in this paper. The stable-state characteristics of the load-side resonant soft-switched single-phase grid-connected inverter are simulated from two cases: normal operation and the presence of sampling delay.

The output current waveforms of the load-side resonant soft-switched single-phase grid-connected inverter under normal operation are shown in Fig. 3. Figure 3(a) shows the waveforms of output currents under PI control, it can be seen that the filtered output current $i_{L2}$ under the PI control strategy suffers from severe oscillatory distortion at about 0.05 s. The waveforms of output currents under PBC in the same conditions are shown in Fig. 3(b). The output current $i_{L1}$ flows in

both directions within the inductor current envelope, which satisfies the zero-voltage conduction conditions of high-frequency switches of BCM modulation, and the waveforms of output current $i_{L2}$ are more stable with lower distortion. It is calculated that the THD of output current after filtering under PI control is 3.4%, while the THD under PBC is 1.7%, so the output current grid integration effect of PBC is better compared with PI control.

The maximum switching frequency of the high-frequency switches in this paper is about 250 kHz according to resonant inductor parameters, so 500 ns is selected as the sampling delay time of the current of resonant inductor. The waveforms of output currents of PI control under the presence of sampling delay of resonant inductor current are shown in Fig. 4(a), and the output current waveforms of PBC under the same condition are shown in Fig. 4(b). From the figure, it can be seen that the waveforms of output currents under PI control have obvious distortion, but the waveforms of output currents under PBC have less distortion, so the passivity-controlled load-side resonant soft-switched single-phase grid-connected inverter has better performance in the presence of resonant sampling current delay.
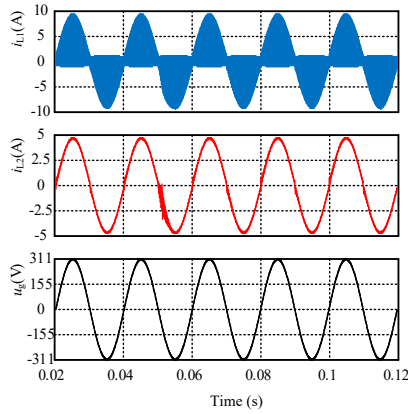


(a) PI
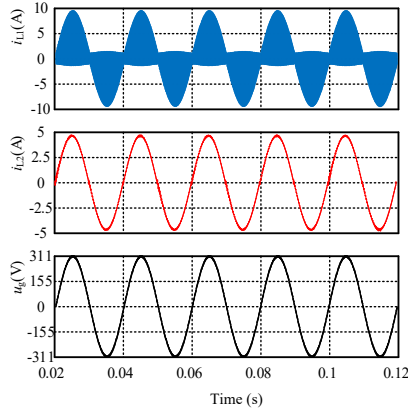
(b) PBC

Fig. 3. Output currents under normal conditions
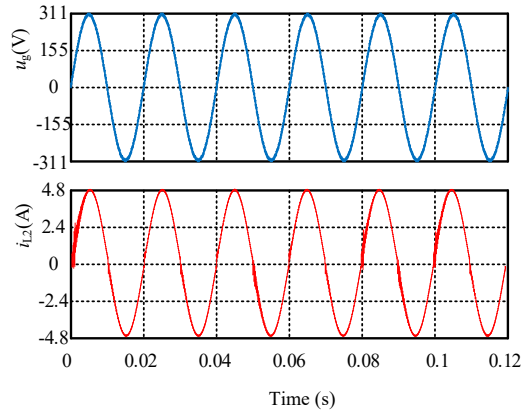


(a) PI
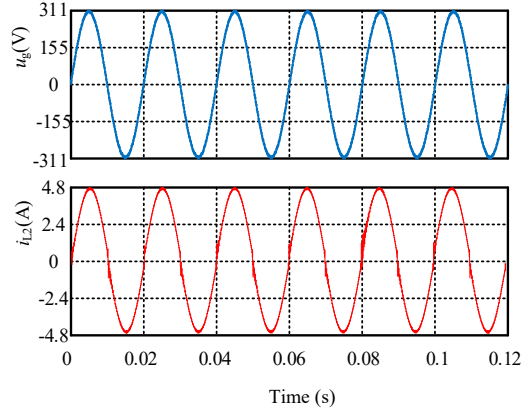
(b) PBC

Fig. 4. Output currents under sampling delay

### 3.6. Dynamic-state simulation analysis

In this paper, the dynamic characteristics are simulated and analyzed in terms of grid voltage dips, grid voltage is distorted by the third and fifth harmonics, grid current surges, and grid phase shifts respectively.

Assuming that the initial peak of grid voltage is 311 V, then the peak of grid voltage drops to 260 V at 0.04 s, the waveforms of output currents under PI control are shown in Fig. 5(a), and the waveforms of output currents under PBC in the same condition are shown in Fig. 5(b). It can be seen from the figure that the peak of output currents under both control methods remain unchanged after the peak of the grid voltage drops after 0.04 s, but the output current waveforms of PI control have a significant local distortion, while the waveform distortion of the output current of PBC is significantly smaller than that of PI control, so the system stability under PBC is better when the grid voltage drops suddenly.

Assuming that the grid voltage is distorted by the third harmonic as well as the fifth harmonic disturbance at 0.04 s, and the content of the third harmonic and the fifth harmonic are 19.2% and 16.1% respectively. The waveforms of output currents under PI control are shown in Fig. 6(a), and the waveforms of output currents under PBC in the same conditions are shown in Fig. 6(b), it can be seen from the figure that the output currents of PBC still maintain good waveforms even if the grid voltage is distorted by harmonic disturbances after 0.04 s, while the output waveforms of the PI control have a more obvious oscillatory distortion near the crossing point, so the load-side resonant soft-switched single-phase grid-connected inverter with the PBC strategy is more resistant to harmonic disturbances.

Assuming that the peak of the desired grid-connected current changes abruptly from 2.4 A to 4.8 A at 45° phase of grid voltage, the output current waveforms of the load-side resonant soft-switched single-phase grid-connected inverter is shown in Fig. 7. It can be seen that when the current changes abruptly as the grid phase is 45°, the PI-controlled waveforms of output currents have a more serious problem of oscillatory distortion past the zero point when the desired current is lower, and a more serious distortion occurs around 0.07 s when the desired current is higher. However, the output current waveforms of PBC not only have no significant distortion when the desired output current is low, but also have a good tracking effect when the desired current



(a) PI                                              (a) PI
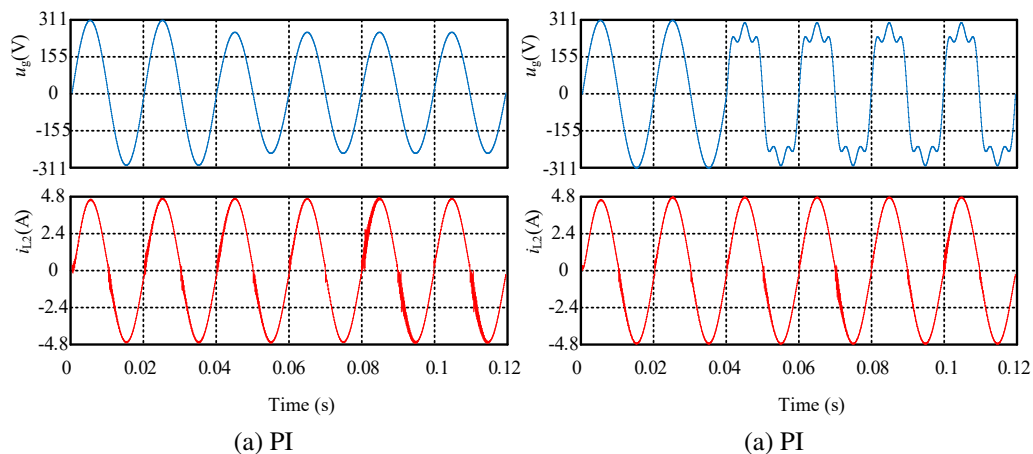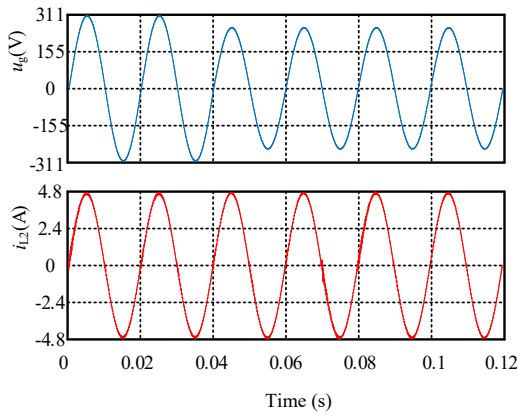
(b) PBC

Fig. 5. Output currents when grid voltage dips
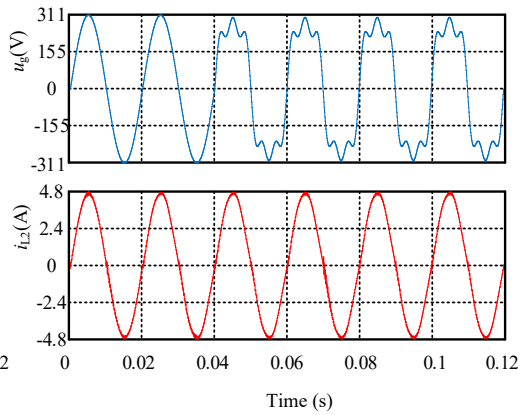
(b) PBC

Fig. 6. Output currents when harmonics occur

occurs in a sudden increase. Therefore, the load-side resonant soft-switching inverter with the PBC strategy has good dynamic performance when the desired output current suddenly increases.

Assuming that the phase of grid voltage is shifted by 45° at 0.045 s, the waveforms of output currents of the load-side resonant soft-switched single-phase grid-connected inverter is shown in Fig. 8. It can be seen that the output currents under both control methods can effectively track the change of phase of the grid voltage when the grid voltage undergoes phase shifts, but the output currents of PBC have a lower distortion degree and better current quality compared with the output current waveforms under PI control, so the load-side resonant soft-switched single-phase grid-connected inverter under passivity-based control is more stable when the phase of grid voltage shifts The stability of the load-side resonant soft-switched single-phase grid-connected inverter with the PBC strategy is therefore stronger when the phase of grid voltage is shifted.
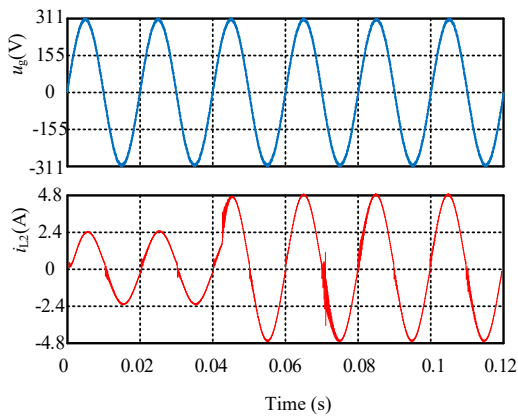


(a) PI
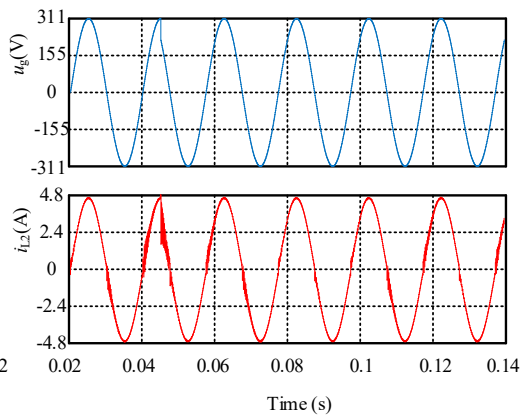
(a) PI
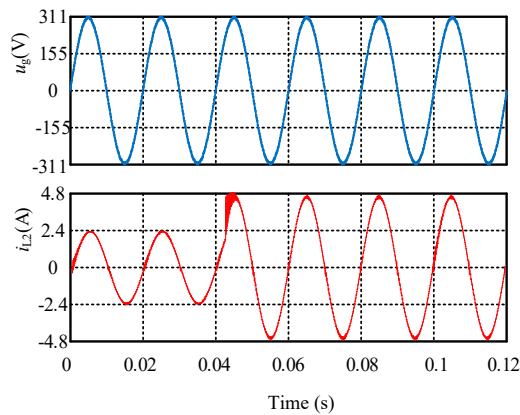
Fig. 7. Output current when it surges
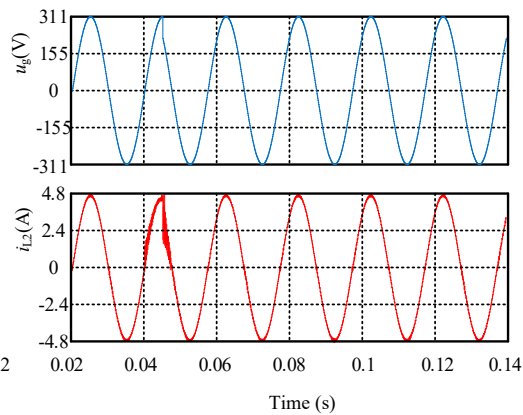
Fig. 8. Output current when grid voltage phase shifts

## 4. Conclusion

In this paper, a PCH model is established and a passivity-based controller is designed based on IDA-PBC theory for a load-side resonant soft-switched single-phase grid-connected inverter, then the passive nature of the system is proved. In addition, this paper builds a load resonant soft-switched grid-connected inverter with the PBC strategy in PSIM software, compares and analyzes it with the traditional PI control from both stable-state and dynamic cases. The simulation results verify that the passivity-based control strategy has increased the stability of system and improved the quality of output waveforms.

### References

[1] Divan D.M., Skibinski G., *Zero-Switching-Loss Inverters for High-Power Applications*, IEEE Transactions on Industry Applications, vol. 25, no. 4, pp. 634–643 (1989), DOI: 10.1109/28.31240.

[2] Park S., Sohn Y., Cho G., *SiC-Based 4 MHz 10 kW ZVS Inverter with Fast Resonance Frequency Tracking Control for High-Density Plasma Generators*, IEEE Transactions on Power Electronics, vol. 35, no. 3, pp. 3266–3275 (2020), DOI: 10.1109/TPEL.2019.2932056.

[3] Khodabandeh M., Afshari E., Amirabadi M., *A Single-Stage Soft-Switching High-Frequency AC-Link PV Inverter: Design, Analysis, and Evaluation of Si-Based and SiC-Based Prototypes*, IEEE Transactions on Power Electronics, vol. 34, no. 3, pp. 2312–2326 (2019), DOI: 10.1109/TPEL.2018.2847242.

[4] Vishnuram P., Ramachandiran G., Ramasamy S., *A Comprehensive Overview of Power Converter Topologies for Induction Heating Applications*, International Transactions on Electrical Energy Systems, vol. 30, no. 10, pp. 1–33 (2020), DOI: 10.1002/2050-7038.12554 .

[5] Ibanez F.M., *Bidirectional Series Resonant DC/AC Converter for Energy Storage Systems*, IEEE Transactions on Power Electronics, vol. 34, no. 4, pp. 3429–3444 (2019), DOI: 10.1109/TPEL.2018.2854924.

[6]    Belkamel H., Kim H., Choi S., *Interleaved Totem-pole ZVS Converter Operating in CCM for Single-Stage Bidirectional AC-DC Conversion with High-frequency Isolation*, IEEE Transactions on Power Electronics, vol. 36, no. 3, pp. 3486–3495 (2021), DOI: 10.1109/TPEL.2020.3016684.

[7]    Amirabadi M., Baek J., *Ultrasparse AC-Link converters*, IEEE Transaction on Industry Applications, vol. 51, no. 1, pp. 448–458 (2015), DOI: 10.1109/TIA.2014.2334736 .

[8]    Chen B., Lai J., Chen C., *Design and Optimization of 99% CEC Efficiency Soft-Switching Photovoltaic Inverter*, 2013 Twenty-Eighth Annual IEEE Applied Power Electronics Conference and Exposition (APEC), Long Beach, USA, pp. 946–951 (2013).

[9]    Qian Z., Haibin H., *A Controlled-Type ZVS Technique Without Auxiliary Components for the Low Power DC/AC Inverter*, IEEE Transactions on Power Electronics, vol. 28, no. 7, pp. 3287–3296 (2013), DOI: 10.1109/TPEL.2012.2225075.

[10]   Ryan R.T., Hogan D.N., Morrison R.J., *Digital Closed-Loop Control Strategy to Maintain the Phase Shift of a Multi-Channel BCM Boost Converter for PFC Applications*, IEEE Transactions on Power Electronics, vol. 34, no. 7, pp. 7001–7012 (2019), DOI: 10.1109/TPEL.2018.2875273.

[11]   Sun J., Li J., Costinett D.J., *A GaN-Based CRM Totem-Pole PFC Converter with Fast Dynamic Response and Noise Immunity for a Multi-Receiver WPT System*, 2020 IEEE Energy Conversion Congress and Exposition (ECCE), Detroit, USA, pp. 2555–2562 (2020).

[12]   Kai Y., Chengjian W., *A Scheme to Improve Power Factor and Dynamic Response Performance for CRM/DCM Buck-Buck/Boost PFC Converter*, IEEE Transactions on Power Electronics, vol. 36, no. 2, pp. 1828–1843 (2021), DOI: 10.1109/TPEL.2020.3007613.

[13]   Boran F., Qiong W., Burgos R., *Adaptive Hysteresis Current Based ZVS Modulation and Voltage Gain Compensation for High-Frequency Three-Phase Converters*, IEEE Transactions on Power Electronics, vol. 36, no. 1, pp. 1143–1156 (2021), DOI: 10.1109/TPEL.2020.3002894.

[14]   Gibong S., Zhengrong H., Qiang Li., *Critical Conduction Mode Based High Frequency Single-Phase Transformerless PV Inverter*, 2020 IEEE Applied Power Electronics Conference and Exposition (APEC), New Orleans, USA, pp. 3232–3237 (2020).

[15]   Haryani N., Sun B., Burgos R., *ZVS Turn-on Triangular Current Mode (TCM) Control for Three Phase 2-Level Inverters with Reactive Power Control*, 2018 IEEE Energy Conversion Congress and Exposition (ECCE), Portland, USA, pp. 4940–4947 (2018).

[16]   Amirahmadi A., Haibing H., Grishina A., *Hybrid ZVS BCM Current Controlled Three-Phase Microinverter*, IEEE Transactions on Power Electronics, vol. 29, no. 4, pp. 2124–2134 (2014), DOI: 10.1109/TPEL.2013.2271302.

[17]   Petrovic V., Ortega R., Stankovic A.M., *Interconnection and damping assignment approach to control of PM synchronous motors*, IEEE Transactions on Control Systems Technology, vol. 9, no. 6, pp. 811–820 (2001), DOI: 10.1109/87.960344.

[18]   Arjan van der Schaft, *L2-gain and passivity techniques in nonlinear control*, Springer-Verlag (1996).

[19]   Jeung Y., Lee D., Dragicevic T., *Design of Passivity-Based Damping Controller for Suppressing Power Oscillations in DC Microgrids*, IEEE Transactions on Power Electronics, vol. 36, no. 4, pp. 4016–4028 (2021), DOI: 10.1109/TPEL.2020.3024716.

[20]   Shengzhao P., Nahid-Mobarakeh B., Pierfederici S., *Interconnection and Damping Assignment Passivity-Based Control Applied to On-Board DC–DC Power Converter System Supplying Constant Power Load*, IEEE Transactions on Industry Applications, vol. 55, no. 6, pp. 6476–6485 (2019), DOI: 10.1109/TIA.2019.2938149.